Novel Parameter Estimation Schemes in Microsystems

Hakan Bilen, Muhammet A. Hocaoglu, Eray A. Baran, Mustafa Unel, Devrim Gozuacik

Abstract— **This paper presents two novel estimation methods that are designed to enhance our ability of observing, positioning, and physically transforming the objects and/or biological structures in micromanipulation tasks. In order to effectively monitor and position the microobjects, an online calibration method with submicron precision via a recursive least square solution is presented. To provide the adequate information to manipulate the biological structures without damaging the cell or tissue during an injection, a nonlinear spring-mass-damper model is introduced and mechanical properties of a zebrafish embryo are obtained. These two methods are validated on a microassembly workstation and the results are evaluated quantitatively.**

I. INTRODUCTION

With the recent advances in micro and nanotechnology, the commercial markets, including microelectromechanical system (MEMS) products such as the key components in automobile airbags, ink-jet printers and projection display systems, have been growing rapidly. Although these commercially available micro devices are currently produced in a batch technique with little assembly, many other products such as read/write heads for hard disks and fiber optics assemblies require flexible precision assemblies [1]. However, the assembly of these products are mostly done in manual or semi-automatic operations. Moreover, many biological micromanipulations such as invitro-fertilization and cell characterization also rely on the ability of human operators. Requirement of high-precision, repeatable and financially viable operations in these tasks has given rise to the elimination of direct human involvement and automation in micromanipulation and microassembly. Dexterous manipulation of microobjects may necessitate calibration of the vision sensors and positioning stages, and controlling the interaction forces.

In the literature, a few groups ([11],[12]) proposed methods to calibrate the optical microscopes coupled with cameras. The calibration of an optical microscope has been carried out by Zhou and Nelson that is based on the Tsai's model, specially modified for the parallel case and experimentally validated [11]. A further method is proposed by Ammi et al. that is based on Zhang's model and modified for a single image [12]. Instead of conventional calibration pattern, a virtual calibration pattern was constructed using a micromanipulator with sub-pixel localization in the image. However, calibrating an optical microscope for each zoom

H. Bilen, M. A. Hocaoglu, E. A. Baran, M. Unel and D. Gozuacik are with the Faculty of Engineering and Natural Sciences, Sabanci University, 34956 Istanbul, Turkey {hakanbil, muhammet, eraybaran}@su.sabanciuniv.edu, {munel,dgozuacik}@sabanciuniv.edu

level individually and thus constructing a look-up table are time consuming. Moreover, a very small change in position or orientation of optical or mechanical components in the workcell requires the reconstruction of the look-up table.

Furthermore, some works ([4]-[6]) characterize the mechanical properties of the involved samples to distinguish the physiological changes and to manipulate biological structures without any harm. In [4], a two-axis cellular force sensor and structural deformations on both mouse oocytes and embryos obtained from a microscope are used to describe the mechanical properties of the mouse zona pellucida based on a biomembrane mechanical model. Same biomembrane model is utilized to understand the evolution of the chorion for the different developmental stages of zebrafish in [5]. However, this model does not consider the dynamical effects due to the velocity and acceleration of the end effector during the injection tasks. Thus, it cannot provide a control on the velocity and the acceleration.

In this work, we develop novel estimators to calibrate the optical and positioning system and to characterize the mechanical properties of the biological structures through a synthesis of concepts from computer vision, estimation and control theory. In order to effectively monitor and position the microobjects, an online calibration method with submicron precision is presented. To provide the adequate information to manipulate the biological structures without damaging the cell or tissue during an injection, a nonlinear spring-mass-damper model is employed.

Section II describes the online optical system calibration and force estimation methods. Section III presents the experimental results and discussions. Finally, Section IV concludes the paper with some remarks.

II. PARAMETER ESTIMATION

A. Online Optical System Calibration

In vision based micromanipulation and assembly applications, transporting mesoscale objects within submicron accuracies and assembling parts at different sizes may require coarse to fine manipulation strategies. During these tasks, the objects may need to be monitored and tracked under different optical magnifications. Thus the optical microscope must be calibrated for each zoom level to effectively use visual feedback in micromanipulation and assembly tasks. Although a look-up table for different optical settings can be generated for each zoom level, constructing a look-up table is time consuming. Therefore an online optical calibration scheme is proposed to overcome the drawbacks of generating a look-up table in this section. Since none of the optical microscope calibration methods ([11],[12]) in the literature can be used
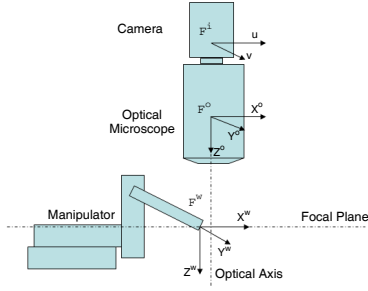
Fig. 1. Image, Objective and World Coordinate Systems

for an online calibration procedure, a new formulation of optical microscope calibration via a recursive least square method is presented.

1) Estimation of Projection Matrix: Fig. 1 illustrates the coordinate systems, objective (F^o), image (F^i) and world (F^w), which are assigned for the online calibration method. The point (o) is the origin of the objective coordinate system whose X^o and Y^o axes are aligned with the rows and columns of image frame respectively. The Z^o axis is aligned with the optical axis of the microscope. The origin of the image coordinate system is intersection of the virtual image plane with the optical axis and u, v axes are parallel to the X^o and Y^o axes. Although the world frame can be assigned arbitrarily, it is more convenient to attach the frame to the tip of the end effector with an orientation in which the axes are chosen to be parallel with the manipulator's motion axes.

The rigid body transformation from the world frame to the objective frame is given by a rotation matrix (R) and a translation vector (T)

$$
\begin{pmatrix} X^o \\ Y^o \\ Z^o \end{pmatrix} = \begin{pmatrix} r_{11} & r_{12} & r_{13} \\ r_{21} & r_{22} & r_{23} \\ r_{31} & r_{32} & r_{33} \end{pmatrix} \begin{pmatrix} X_w \\ Y_w \\ Z_w \end{pmatrix} + \begin{pmatrix} T_x \\ T_y \\ T_z \end{pmatrix} \quad (1)
$$

The coordinates of a point (X^o, Y^o, Z^o) in the objective frame and its projection in the image frame (u, v) can be related as follows,

$$
\begin{aligned}
u &= \frac{f}{s_x} \frac{X^o}{Z^o} + o_x \\
v &= \frac{f}{s_y} \frac{Y^o}{Z^o} + o_y
\end{aligned} \quad (2)
$$

where f is the objective focal length, s_x and s_y are horizontal and vertical pixel sizes respectively. (o_x, o_y) is the principal point which is assumed to be center of the CCD array. Plugging the equation (1) into (2) gives

$$
\begin{aligned}
u - o_x &= f_x \frac{r_{11}X^w + r_{12}Y^w + r_{13}Z^w + T_x}{r_{31}X^w + r_{32}Y^w + r_{33}Z^w + T_z} \\
v - o_y &= f_y \frac{r_{21}X^w + r_{22}Y^w + r_{23}Z^w + T_y}{r_{31}X^w + r_{32}Y^w + r_{33}Z^w + T_z}
\end{aligned} \quad (3)
$$

where $f_x = f/s_x$ and $f_y = f/s_y$. Assuming that the object plane is nearly parallel with the image plane, i.e. $r_{13} = r_{23} = r_{31} = r_{32} \simeq 0$ and $r_{33} \simeq 1$, (4) can be rewritten as follows,

$$
\begin{aligned}
u - o_x &= f_x \frac{r_{11}X^w + r_{12}Y^w + T_x}{Z^w + T_z} \\
v - o_y &= f_y \frac{r_{21}X^w + r_{22}Y^w + T_y}{Z^w + T_z}
\end{aligned} \quad (4)
$$

Since the depth of microobjects are usually much smaller than the mean distance ($\overline{Z}$) along the optical axis, the image

coordinates of an object can be written in the objective frame as

$$
\begin{aligned}
u - o_x &\approx f_x \frac{X^o}{\overline{Z}} = M_x(r_{11}X^w + r_{12}Y^w + T_x) \\
v - o_y &\approx f_y \frac{Y^o}{\overline{Z}} = M_y(r_{21}X^w + r_{22}Y^w + T_y)
\end{aligned} \quad (5)
$$

where $M_x = \frac{f_x}{\overline{Z}}$ and $M_y = \frac{f_y}{\overline{Z}}$ are the magnifications along the x and y axes of the objective.

The relationship between the (X^w, Y^w) coordinates of a point in space and (u, v) coordinates of its projection on the image plane can be written by employing a 2×3 projection matrix P,

$$
\begin{pmatrix} u_i \\ v_i \end{pmatrix} = P \begin{pmatrix} X_i^w \\ Y_i^w \\ 1 \end{pmatrix} \quad (6)
$$

where $P \in \Re^{2 \times 3}$.

Equation (6) can be recast linearly in terms of the entries of P matrix as follows:

$$
y = \varphi^T \theta \quad (7)
$$

where $y = \begin{pmatrix} u_i \\ v_i \end{pmatrix}$, $\varphi = \begin{pmatrix} X_i^w & Y_i^w & 1 & 0 & 0 & 0 \\ 0 & 0 & 0 & X_i^w & Y_i^w & 1 \end{pmatrix}^T$ and $\theta = \begin{pmatrix} p_{11} & p_{12} & p_{13} & p_{21} & p_{22} & p_{23} \end{pmatrix}^T$.

In order to solve for the parameter vector θ, φ matrix has to be nonsingular. Thus, one can assign three points with known world and image coordinates to provide a square φ matrix.

Having supposed that only world and image coordinates of a single point is available in each iteration, the regressor matrix φ can be augmented with two previous measurements to provide a square matrix. Assuming that transformation parameters are constant for three consecutive frames, (7) can be rewritten as follows:

$$
\underbrace{\begin{pmatrix} y_k \\ y_{k-1} \\ y_{k-2} \end{pmatrix}}_{y} = \underbrace{\begin{pmatrix} \varphi_k^T \\ \varphi_{k-1}^T \\ \varphi_{k-2}^T \end{pmatrix}}_{\varphi^T} \underbrace{\begin{pmatrix} p_{11} \\ p_{12} \\ p_{13} \\ p_{21} \\ p_{22} \\ p_{23} \end{pmatrix}}_{\theta} \quad (8)
$$

where the redefined $y \in \Re^6$ and $\varphi \in \Re^{6 \times 6}$.

Suppose that the observed data actually have been generated by (8), we can define our predictor as,

$$
\hat{y}(t|\theta) = \varphi(t)^T \hat{\theta}(t) \quad (9)
$$

In light of (9) the prediction error becomes

$$
\varepsilon(t, \theta) = \varphi(t)^T \theta(t) - \varphi(t)^T \hat{\theta}(t) \quad (10)
$$

In order to evaluate the magnitude of the prediction error, we can define a norm for $\varepsilon(t, \theta)$ as

$$
V_N(\theta, Z_N) = \frac{1}{N} \sum_{t=1}^{N} \ell(\varepsilon(\theta, t) = \frac{1}{N} \sum_{t=1}^{N} \frac{1}{2}\beta(N, t)[y(t) - \varphi^T(t)\theta]^2 \quad (11)
$$

2395

V_N can be modified by adding a regularization term as follows

$$V_N(\theta) = \frac{1}{N}\sum_{t=1}^{N}\frac{1}{2}\beta(N,t)([y(t)-\varphi^T(t)\theta]^2 + \delta \parallel \theta - \theta^0 \parallel^2) \tag{12}$$

where, $\beta(N,t)$ is a weighting function and δ is the regularization parameter. The estimate that minimizes the criterion in (12) is formally given as

$$\hat{\theta}_t = \arg\min \sum_{t=1}^{N}\frac{1}{2}\beta(N,t)([y(t)-\varphi^T(t)\theta]^2 + \delta \parallel \theta - \theta^0 \parallel^2) \tag{13}$$

This estimate is computed as follows:

$$\hat{\theta}_t = \overline{R}^{-1}(t)f(t) \tag{14}$$

where

$$\overline{R}(t) = \sum_{k=1}^{t}\beta(t,k)[\varphi(k)\varphi^T(k)+\delta I] \tag{15}$$

and,

$$f(t) = \sum_{k=1}^{t}\beta(t,k)[\varphi(k)y(k)+\delta\theta^0] \tag{16}$$

Equations (14)-(16) can be rewritten recursively as

$$\hat{\theta}_t = \hat{\theta}_{t-1} + \overline{R}^{-1}(t)f(t) \tag{17}$$

$$\overline{R}(t) = \lambda(t)\overline{R}(t-1) + \varphi(t)\varphi^T(t) + \delta I \tag{18}$$

$$f(t) = \lambda(t)f(t-1) + \varphi(t)y(t) + \delta\theta^0 \tag{19}$$

2) Computing Optical System Parameters: Having recovered the projection matrix P from the estimate θ, the entries of the projection matrix can now be related to the intrinsic and extrinsic optical system parameters by using (4) and (5),

$$P = \begin{pmatrix} M_x r_{11} & M_x r_{12} & M_x T_x \\ M_y r_{21} & M_y r_{22} & M_y T_y \end{pmatrix} \tag{20}$$

Since the image center (o_x, o_y) is assumed to be known, it is not explicitly shown in (20). Assuming that the aspect ratio $(\alpha = s_y/s_x)$ is unity, $(r_{11}, r_{12}, r_{21}, r_{22})$ can be obtained up to a scale. Because any scaled $(r_{11}, r_{12}, r_{21}, r_{22})$ must correspond to only a single rotation matrix, the three rotation angles, T_x, T_y and magnification can be computed.

B. Force Estimation

Dexterous micromanipulation operations usually demand monitoring, positioning and transforming skills. Although, some successful experiments with only monitoring and positioning objects were reported in [2], [3], [8] and [9], more complex manipulation scenarios call for an additional force information to provide high dexterity. In biomanipulation tasks, acquiring the force information is specifically important to ensure successful operations without damaging the biological structures. However, the requirement of measuring forces between the range from 1 mN down to 1 μN and below poses challenges on the design and construction of force sensors [7]. Although force measurements can be done by using strain gauges, piezoelectric, capacitive sensors or

laser-based optical techniques in micromanipulation operations, microforce sensing is still an open and developing research field. The integration of microforce sensors with end effectors such as micropipettes is very challenging and costly due to the complex fabrication and assembly techniques. Therefore, once the object to be manipulated is mechanically characterized with the measurements from a force and vision sensor, the estimated parameters can be employed to reconstruct the imposing forces for the future manipulation tasks by using only the existing optical microscope and CCD camera.

1) Estimation Model: We propose a new approach to estimate the mechanical properties of cellular structures which uses vision and force information. In this method, not only the static but also dynamic effects are considered using a nonlinear mass-spring-damper model. Thus, the computed parameters can be utilized to estimate the imposed force on a biomembrane and provide the adequate information to control the position, velocity and acceleration of the probe without damaging the cell or tissue during a micromanipulation task.

The one dimensional mass-spring-damper model with a hardening spring is given as,

$$F = m\ddot{x} + b\dot{x} + k_1 x + k_2 x^3 \tag{21}$$

where F is the applied force, m, b, k_1 and k_2 are the mass, damping, first and second spring coefficients of the object which is being manipulated. Assuming that the applied force, acceleration, velocity and position of the object are known, (21) can be rewritten linearly in terms of the unknown m, b, k_1 and k_2 parameters as follows,

$$F = \underbrace{\begin{pmatrix} \ddot{x} & \dot{x} & x & x^3 \end{pmatrix}}_{\varphi^T}\underbrace{\begin{pmatrix} m \\ b \\ k_1 \\ k_2 \end{pmatrix}}_{\theta} \tag{22}$$

Since measuring the force for multiple points in each iteration with a single force sensor output is not possible, assuming that the unknown parameters are constant for at least four time steps, φ can be expanded to a square or overdetermined matrix by concatenating force and deformation measurements from these time steps,

$$\begin{pmatrix} F_n \\ F_{n-1} \\ F_{n-2} \\ F_{n-3} \end{pmatrix} = \underbrace{\begin{pmatrix} \varphi_n^T \\ \varphi_{n-1}^T \\ \varphi_{n-2}^T \\ \varphi_{n-3}^T \end{pmatrix}}_{\varphi^T}\underbrace{\begin{pmatrix} m \\ b \\ k_1 \\ k_2 \end{pmatrix}}_{\theta} \tag{23}$$

where n is the nth time step, $\varphi_i = \begin{pmatrix} \ddot{x}_i & \dot{x}_i & x_i & x_i^3 \end{pmatrix}^T$ and the redefined $\varphi \in \Re^{4\times4}$.

Although θ vector can be solved with the standard least squares, φ may be ill-conditioned or yielding many solutions. In order to compute θ with desirable properties, the cost function is given with a regularization term,
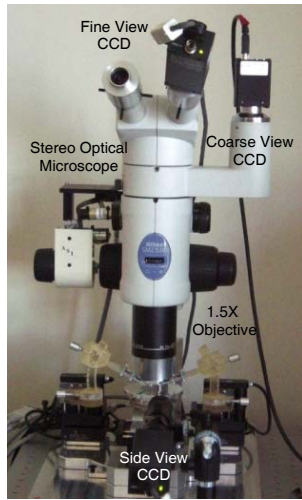
2396

Fig. 2. Vision Hardware of Workstation

Fig. 3. Sample and Manipulator Stages

$$\varepsilon = \parallel F - \varphi^T \theta \parallel^2 + \delta \parallel \theta - \theta^0 \parallel^2 \qquad (24)$$

where δ is a positive scalar. Adding the regularization term $\delta \parallel \theta - \theta^0 \parallel^2$ to the linear regression improves the robustness of the algorithm. Since the force and the spatial measurements are often distorted by noise, the regularization may enhance the condition number of φ matrix. Assuming θ^0 is the origin, an explicit solution, denoted by $\hat{\theta}$, is given as,

$$\hat{\theta} = (\varphi\varphi^T + \delta I)^{-1} \varphi F \qquad (25)$$

where $I \in \Re^{4 \times 4}$ is the identity matrix.

III. EXPERIMENTAL RESULTS

A. Hardware Setup

The experiments were conducted on the microassembly workstation shown in Fig. 2. In the microassembly workstation different magnification and resolution levels are available. In order to allow global and local visual information, a coarse and a fine view with variable zooming are employed. These cameras are mounted on a stereo optical microscope, Nikon SMZ1500 with 1.5x objective and 0.75:11.25 zoom ratio. The vision system is shown in Fig. 2.

Since optical microscopes suffer from the low depth of field which limits the focal plane into a small range and causes defocused view of the object monitored outside this region, a lateral microscope with an additional CCD camera is employed to acquire the height information for the interested object.

It is also important to accurately handle the micro parts for a dexterous manipulation, since the micro parts to be manipulated are usually fragile. Therefore two types of end effectors, a probe and a microgripper which are integrated with capacitive force sensors were used. Both of the gripper and the probe are products of FEMTOTOOLS® and are able to sense the forces with a resolution down to 0.4 μN and 0.01 μN respectively. The force sensing probe and gripper are mounted on tilted holders to reach the desired point effectively. An illustrative figure is given in Fig. 3. The force sensing probe
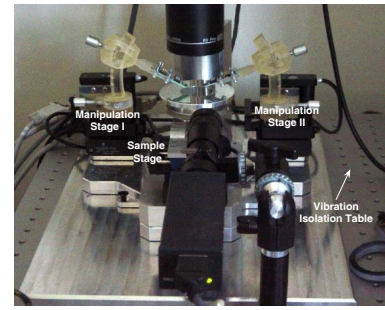
and gripper are mounted on two separate 3-DOF fine positioning stages with effective x-y-z range of 15x15x15 mm and 50 nm closed loop precision. On an x-y-θ positioning stage, with effective x-y range of 15x15 mm, 50 nm close loop precision, and 4.5×10^{-5} degrees rotation resolution, a glass slide is mounted and positioned under the force sensing probe and microgripper. The high precision positioning stages are depicted in Fig. 3.

B. Online Optical System Calibration Results

The online calibration algorithm is implemented on the microassembly workstation to show the validity of the presented method. A square pattern on the sample stage is moved along a circular path in the x-y plane and one of its corner is tracked in subpixel accuracy at 30 Hz. Along the designed trajectory, the magnification is changed from 0.9X to 1.2X at the 45th iteration. Pixel coordinates of the image feature along the encoder output of the sample stage are used to test the online parameter estimation algorithm. The trajectory which is followed by the corner in the image and world coordinates are depicted in Fig. 4.
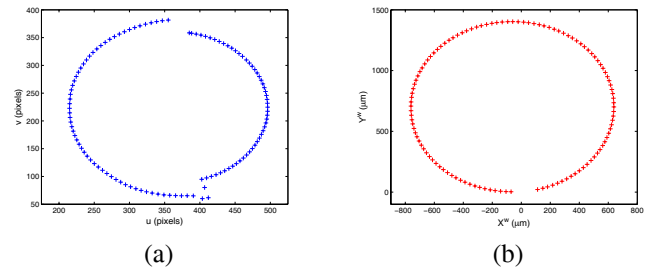

(a)

(b)

Fig. 4. The Trajectory of the Corner in (a) Image and (b) World Coordinates. In (a), the small and larger semicircular trajectories imply 0.9X and 1.2X respectively

Using the obtained trajectory information in the online parameter estimation algorithm, the entries of the projection matrix are computed and shown in Fig. 5.

The evolution of the prediction error in (10) is computed using the estimated projection matrix, plotted in Fig. 6.

It is shown that the prediction error decays to 0.1 pixels after the magnification change after 8 iterations. Once we have the projection matrix, we can obtain the optical system parameters using (20). The computed magnification during the experiment is depicted in Fig. 7.

It is observed that the proposed method converges to the new magnification value in 8 steps or 0.26 seconds. It is also noticed that there exists a jump in the computed magnification during the magnification change. Since the collected world and image coordinates during the transition imply different projection matrices and intrinsic parameters, the augmented φ may be ill-conditioned and result in wrong parameters. Therefore, the forgetting factor β is automatically increased to eliminate the effect of the past data, once the magnification motor turns. The convergence time could also be
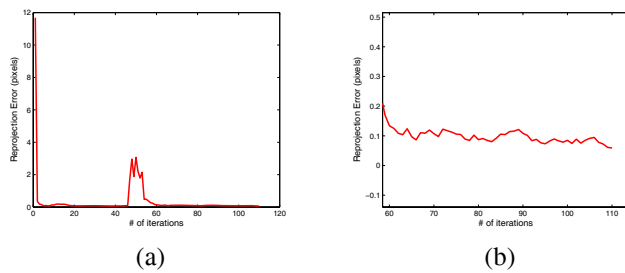
2397
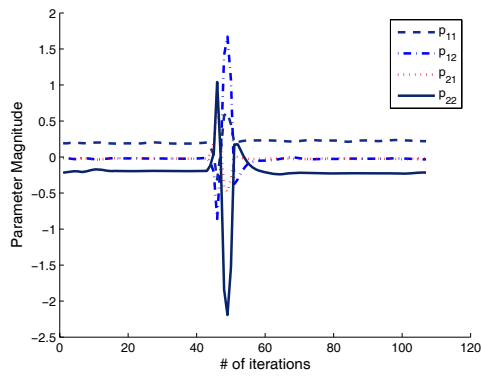
(a)
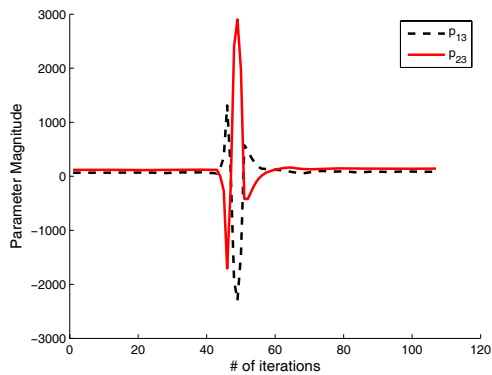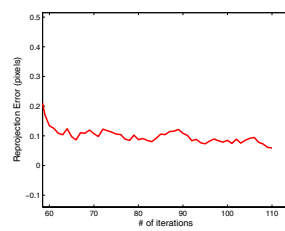

(b)

Fig. 5.   Estimated Entries of the Projection Matrix
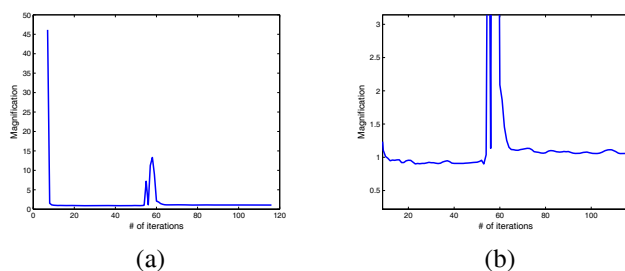

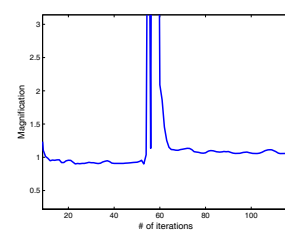(a)   (b)

Fig. 6.   (a) Prediction Error (b) Zoomed Prediction Error

(a)   (b)

Fig. 7.   (a) Computed Magnification Plot (b) Zoomed Magnification Plot

improved by increasing the speed of the magnification motor and thus providing a step response.

Note that there exist small variations in the computed magnification. Since the camera and the manipulator frames are not perfectly aligned, the Z coordinate of the moving center in the objective frame

may alter in a small range without that the image is getting blurred. Therefore, the calibration parameters can be modified during the motion.

C. Force Estimation Results

In order to evaluate the performance of the force estimation model, zebrafish embryos are chosen to be experimented. Due to its easily accessible eggs, high fertility, external fertilization and translucent embryos, zebrafish is preferred. In addition, zebrafish embryos have a delicate structure and small forces may create significant deformations on their membranes which is desirable for testing the proposed model in spite of their relatively large size $(1.2 - 1.4$ mm$)$. After the freshly harvested eggs are put on the sample stage in a petridish, a microgripper is employed to immobilize the embryo during the compression. Before the force sensing probe applies a uniaxial load compressing the biomembrane, the probe is aligned with the embryo in a way that the tangential forces are eliminated. An illustrative scene is shown in Fig. 8.
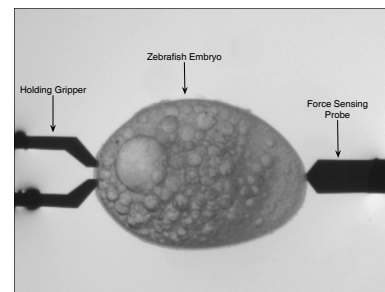

Fig. 8.   Zebrafish Embryos with Holding Gripper and Force Sensing Probe

The experiments are conducted in room temperature (22-24°C). The force and deformation measurements are obtained at 30 Hz during the force loading. The probe moves to the center of the egg at 5 $\mu m/s$ before the force reaches to the maximum of force sensing range and then returns to its initial position at the same velocity. Note that the acceleration of the contact point is zero except the direction changes. Thus, the acceleration and the mass of the probe are not computed in the experiments. The force information is obtained from the capacitive force sensor embedded in the probe. The deformation and velocity of the contact point are calculated by the Lucas-Kanade optical flow estimation method [13] with subpixel accuracy.

The resulting force for the trapezoid displacement is illustrated in Fig. 9.
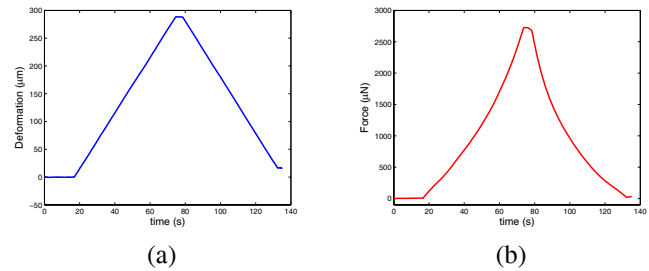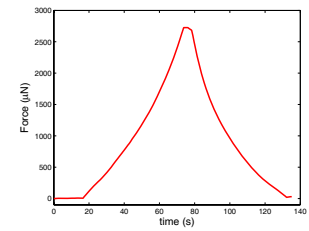
(a)   (b)

Fig. 9.   (a) Deformation (b) Force

Having measured the force during the experiment, the explicit solution in (25) gives the parameters as $\hat{k}_1 = 4.5161, \hat{k}_2 = 0.0001, \hat{b} = 27.7200$. Although this estimation results in 3.89 percent error, modeling the second part of the force (after the velocity is negative) with the same spring-mass-damper parameters may be inaccurate from a robotics point of view. Neglecting the damping effects in the second part, the unknown parameters can be estimated by fitting

2398

only the second part of force data to a mass-spring model. The damping coefficient can be obtained by relating the error with the velocity in the first part. The estimation yields the parameters, $\hat{k}_1 = 2.9577, \hat{k}_2 = 0.0001, \hat{b} = 51.3317$ with a 5.22 percent error. The reconstructed force with the estimated parameters for first and second parts are respectively shown in Fig. 10.
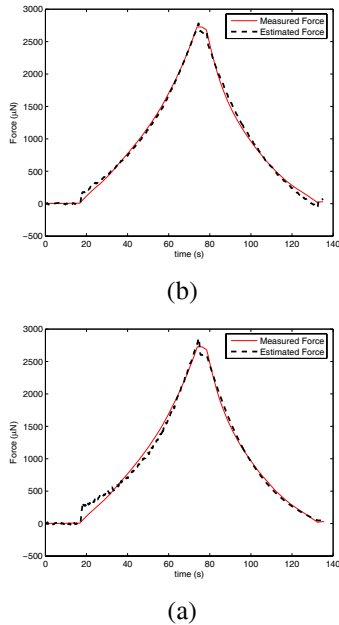

Fig. 10. Measured and Reconstructed Force for First Part (a) and Second Part (b)

We can also fit the first part of the measured force into the model, estimate the three parameters and reconstruct the force by using three parameters for the first part and assuming $b = 0$ for the second part. The error between the measured and estimated force is 10.72 percent of the measured one. However, this method yields poor estimation result in the second part. This result may be explained with the observation that the membrane of the embryo is not recovering to its original position at the end of the manipulation. 25 micron offset is observed between the position of the contact point in the first and the last frame. The reason for that offset can be due to the fact that the holding gripper may be penetrated into the embryo, while the probe is pushing the embryo. This offset can be eliminated by modifying the displacement $x(t)$ as

$$x^*(t) = x(t) - 25(1 - e^{-\alpha t}) \quad (26)$$

which means that the offset gradually becomes 25 microns. The estimated forces before and after the displacement elimination are shown in Fig. 11 respectively.

The error becomes 3.6 percent of the measured force with the parameters $\hat{k}_1 = 5.8781, \hat{k}_2 = 3.8346e - 5, \hat{b} = 1.1834$.

IV. CONCLUSION

We have now presented two estimation schemes to enhance the existing manipulation skills in the micro domain. Firstly, an online optical system calibration approach is proposed to improve the precision of the visually guided manipulations. Secondly, a force reconstruction method which is modeled by a nonlinear spring-mass-damper model is presented to control the interaction forces between the manipulator and the object. These methods are experimentally validated using the presented microassembly workstation.
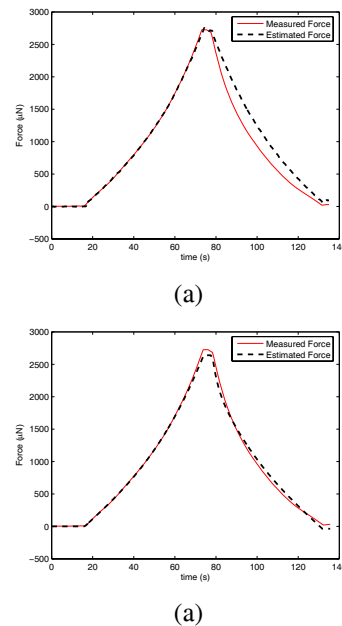

Fig. 11. Measured and Reconstructed Force Before (a) and After (b) Displacement Elimination

V. ACKNOWLEDGEMENT

REFERENCES

[1] B. Kim, H. Kang, D.H. Kim, G.T. Park, J.O. Park, "Flexible Microassembly System based on Hybrid Manipulation Scheme", *IEEE/RSJ Int. Conf. on Intelligent Robots and Systems*, Nevada, 2003, pp. 2061–2066.
[2] G. Yang, J.A. Gaines, B.J. Nelson, "A flexible experimental workcell for efficient and reliable wafer-level 3D micro-assembly", *IEEE Int. Conf. Robotics and Automation*, 2001, vol.1, pp. 133–138.
[3] Y. Sun, B.J. Nelson, "Microrobotic cell injection", *Int. Conf. on Robotics and Automation*, 2001, vol.1, pp. 620–625.
[4] Sun, Y. Wan, Kenneth, R.P., Bischof, J.C. and Nelson, B.J. Member, "Mechanical property characterization of mouse zona pellucida", *IEEE Trans. on Nanobioscience*, 2003, vol. 2, no. 4, pp. 279–286.
[5] D.-H. Kim, C.N. Hwang, Y. Sun, S.H. Lee, B. Kim, B.J. Nelson, "Mechanical Analysis of Chorion Softening in Prehatching Stages of Zebrafish Embryos", *IEEE Trans. on Nanobioscience*, 2006, vol. 5, no. 2, pp. 89–94.
[6] W.H.Wang, X.Y. Liu, Y. Sun, "Autonomous Zebrafish Embryo Injection Using a Microrobotic System", *Int. Conf. on Automation Science and Engineering*, 2007, pp. 363–368.
[7] Z. Lu, P.C.Y. Chen, W. Lin, "Force Sensing and Control in Micromanipulation", *IEEE Trans on Systems, Man, and CybernaticsPart C: Applications and Reviews*, 2006, vol. 36, NO. 6, pp. 713–724.
[8] T. Kasaya, H. Miyazaki, S. Saito, T. Sato, "Micro object handling under SEM by vision-based automatic control", *IEEE Int. Conf. Robotics and Automation*, Detroit, 1999, pp. 2189-2196.
[9] D. H. Kim, Y. Kim, K. Y. Kim, and S. M. Cha, "Dexterous teleoperation for micro parts handling based on haptic/visual interface", *IEEE Int. Symp. Micromechatron. Human Sci.*, 2001, pp. 211-217.
[10] L. Ljung: "System Identification - Theory For the User", 2nd ed, PTR Prentice Hall, Upper Saddle River, N.J., 1999.
[11] Y. Zhou, B.J. Nelson, "Calibration of a parametric model of an optical microscope", *Optical Engineering*, 1999, vol. 38, pp. 1989–1995.
[12] Ammi, M., Fremont, V., Ferreira, A. "Flexible Microscope Calibration using Virtual Pattern for 3-D Telemicromanipulation", 2005, *IEEE Trans. on Robotics and Automation*, pp. 3888–3893.
[13] B.D. Lucas, T. Kanade, "An iterative image registration technique with an application to stereo vision", *Imaging Understanding Workshop*, 1981, pp 121–130.

2399